Position detection and observation of a conducting filament hidden under a top electrode in a Ta_2O_5-based atomic switch

2015 Nanotechnology 26 145702

(http://iopscience.iop.org/0957-4484/26/14/145702)

IOP Publishing Nanotechnology
Nanotechnology 26 (2015) 145702 (7pp) doi:10.1088/0957-4484/26/14/145702

Position detection and observation of a conducting filament hidden under a top electrode in a Ta_2O_5-based atomic switch

Alpana Nayak[1,2], Qi Wang[1,2], Yaomi Itoh[1,2], Tohru Tsuruoka[1,2], Tsuyoshi Hasegawa[1,2], Liam Boodhoo[3], Hiroshi Mizuta[3] and Masakazu Aono[1]

[1] WPI Center for Materials Nanoarchitectonics, National Institute for Materials Science, 1-1 Namiki, Tsukuba, Ibaraki 305-0044, Japan
[2] Japan Science and Technology Agency, CREST, 5 Sanbancho, Chiyoda-ku, Tokyo, 102-0075, Japan
[3] Nano Research Group, Electronics and Computer Science, University of Southampton, Southampton, SO17 1BJ, UK

E-mail: HASEGAWA.Tsuyoshi@nims.go.jp

Received 5 January 2015, revised 18 February 2015
Accepted for publication 18 February 2015
Published 16 March 2015

Abstract

Resistive random access memories (ReRAMs) are promising next-generation memory devices. Observation of the conductive filaments formed in ReRAMs is essential in understanding their operating mechanisms and their expected ultimate performance. Finding the position of the conductive filament is the key process in the preparation of samples for cross-sectional transmission electron microscopy (TEM) imaging. Here, we propose a method for locating the position of conductive filaments hidden under top electrodes. Atomic force microscopy imaging with a conductive tip detects the current flowing through a conductive filament from the bottom electrode, which reaches its maximum at a position that is above the conductive filament. This is achieved by properly biasing a top electrode, a bottom electrode and the conductive tip. This technique was applied to Cu/Ta_2O_5/Pt atomic switches, revealing the formation of a single Cu filament in a device, although the device had a large area of $5 \times 5\ \mu m^2$. Change in filament size was clearly observed depending on the compliance current used in the set process. It was also found from the TEM observation that the cross-sectional shape of the formed filament varies considerably, which is attributable to different Cu nuclei growth mechanisms.

Keywords: resistive random access memories, conductive filament, atomic switch, AFM, TEM

(Some figures may appear in colour only in the online journal)

1. Introduction

Resistive random access memories (ReRAMs) are promising next-generation memory devices [1, 2]. There are several types of ReRAMs [3], such as oxygen vacancy-based ReRAMs [4] and cation-based ReRAMs [5]. It is widely believed that in the former type, oxygen vacancy drift is controlled, such as in TiO_x [6, 7], TaO_x [8, 9], NiO_x [10], and HfO_x [11], where an oxygen deficient region becomes a conductive channel. In the latter type, metal cation (e.g. Ag^+ and Cu^{Z+}) drift is controlled, such as in Ta_2O_5 [12, 13] and SiO_2 [14, 15], where a metal filament is formed. However, the local structure of conductive filaments is still controversial. For instance, some of the major concerns in this field of research are estimating the number and thickness of filaments that are formed in a device [16], and whether a conductive path consists of a continuous filament or a chain of metal clusters [15]. Since the answer depends on a particular system as well as the specific operating conditions, observations of conductive channels are required for each and every system to completely reveal their characteristics.

Several techniques have been reported for finding the positions of conductive filaments [17]. One such technique uses an atomic force microscopy (AFM) conductive cantilever as the ReRAM top electrode, where the conductive cantilever scans over the metal oxide layer that is not covered by a top electrode [18]. This method has enabled dynamic observation of the evolution of metal filaments, both in a set process and in a reset process. In addition, the scanned conductive cantilever works as multiple electrodes, resulting in the formation of a plurality of filaments. Although it is said that the formation of multiple filaments occurs even in conventional device structures [19], another technique is required to confirm this.

The most promising method is to find the position of a conductive filament after setting the device in actual operating mode, i.e., with use of a top electrode, following which, the position is cut out from the device for cross-sectional transmission electron microscopy (TEM) observation. Another method that has been reported is to dig into the top electrode using a hard and conductive (e.g., doped-diamond) cantilever, then, the position is located by detecting the current flowing through the conductive filament from the bottom electrode through the use of a bias that is sufficiently small that it does not cause additional filament formation [20]. Although this method is simple, information on the interface between the conductive filament and the top electrode is lost. To date, one novel technique has been reported that can find the position of a conductive filament without removing the top electrode [21]. This technique uses a small (atomic) force to modify the conductivity of the filament. Only when, the tip-apex of the cantilever is above a filament, the filament is locally distorted and its conductivity is slightly modified. For TaO_x-based ReRAMs, this method successfully revealed that the conductive filament consists of an oxygen deficient region. We also applied this technique to atomic switches, where metal cations should form a conductive filament. However, no modification in conductance was detected. This may be because the small force applied by the cantilever to the metal filament causes a change in conductivity that is too small to be detected. Here, we propose a method for finding the position of a conductive filament through a top electrode by properly biasing a top electrode, a bottom electrode and a conductive cantilever.

The $Cu/Ta_2O_5/Pt$ atomic switch is a system that has been well studied in recent years. In addition to standard ON/OFF bi-stable switching operation [12, 22, 23], it also demonstrated memristive operation, quantized conductance and biological synaptic behavior [24]. The materials and the fabrication process for this type of atomic switch are compatible with those of current complementary metal–oxide–semiconductors (CMOS), which enables them to be integrated with CMOS circuits [25]. Since switching mechanisms have great potential for technological applications, an understanding of their microscopic details is essential. Our earlier studies, based mainly on current–voltage measurements, suggested that the key factor in switching is metal filament formation and annihilation. However, direct observations of metal filaments have not yet been achieved because of the difficulty in finding their actual position inside the devices due to the presence of the top electrode.

2. Experimental

The $Cu/Ta_2O_5/Pt$ devices were fabricated on SiO_2/Si substrates. The thicknesses of the Cu, Ta_2O_5 and Pt layers were 20, 15–20, and 30 nm, respectively. To prevent oxidation, an additional layer of Pt (5 nm) or Au (30 nm) was deposited over the top Cu electrode. Ta_2O_5 was deposited by RF sputtering. All other metal layers were deposited by electron-beam deposition. All depositions were achieved at room temperature, and metal masks were used during deposition for patterning. The preparation details are reported elsewhere [12]. The device size was $5 \times 5\ \mu$m.

The devices were switched-on by sweeping bias between the top (Cu) and bottom (Pt) electrodes using a system source meter (Keithley 2611B), where the top electrode was grounded. The AFM measurements were done at room temperature and ambient conditions using a JEOL-SPM head controlled by a Nanonis system. A conductive cantilever (a Pt tip was mounted using a focused ion beam (FIB) technique on a commercially available cantilever (Olympus, OMCL-AC240TM-R3)) was used to detect the local current by biasing the cantilever at 1 mV and the bottom electrode at −150 mV or −500 mV while the top electrode was grounded. After mounting, the apex of a Pt tip was sharpened by FIB to a radius of about 10 nm, resulting in a resolution of about 10 nm in the *xy*-plane direction and of about 1 nm in the *z*-direction. SEM images of a Pt tip are shown in figure 1(a). The top electrode of our device exhibits roughness on the order of a few nm, which was confirmed by TEM cross-sectional observation. Prior to the experiments on the devices, the conductivity of the cantilever was checked by linear *I*/*V*s measured on a metal (Pt) surface. This is schematically shown in figure 1(b). Since a metal filament would be highly conductive, the resistance of the metal filament (R_{CF}) can be smaller than the resistance of the top electrode (R_{top}) and the bottom electrode (R_{bottom}) in the measured system. The resistance of the electrodes in our device is typically on the order of 100 Ω. An equivalent circuit of the measurement system is shown in figure 1(c), where R_{CONT} corresponds to the contact resistance between the Pt tip of the cantilever and the top electrode. Since R_{CONT} is on the order of 1 MΩ in our measurements, major current flows in the bottom loop of the equivalent circuit. In other words, the distribution of electric potential (ϕ) on the top electrode does not change as a dependence of the position of the cantilever. Namely, electric potential (ϕ) becomes maximum at the top of the conductive filament, resulting in the maximum current flowing through the conductive cantilever, as schematically shown in figure 1(d). By detecting the maximum point of current flowing through the cantilever, we can detect the position of the conductive filament.

To confirm metal filament formation, high-resolution TEM and energy dispersive x-ray (EDX) mapping were carried out using HD-2300 (Hitachi High-Technologies).

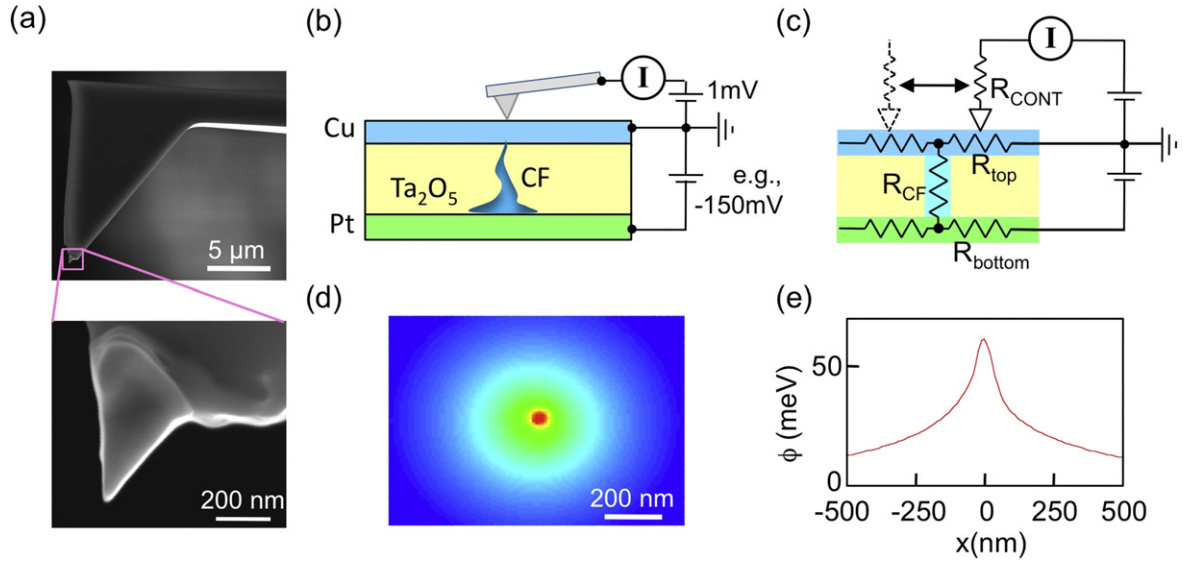

Figure 1. (a) SEM images of a FIB sharpened Pt tip. (b) Schematic of the measurement set up using a conductive-AFM Pt-tip and a Cu/Ta_2O_5/Pt device to locate the position of a conducting filament. (c) Equivalent circuit of the measurement. (d) Electric potential map of a top electrode, the center of which is the filament position. Calculations were done by assuming that −150 mV is applied to a bottom electrode. (e) Line profile of electric potential as a function of the distance from the filament position.

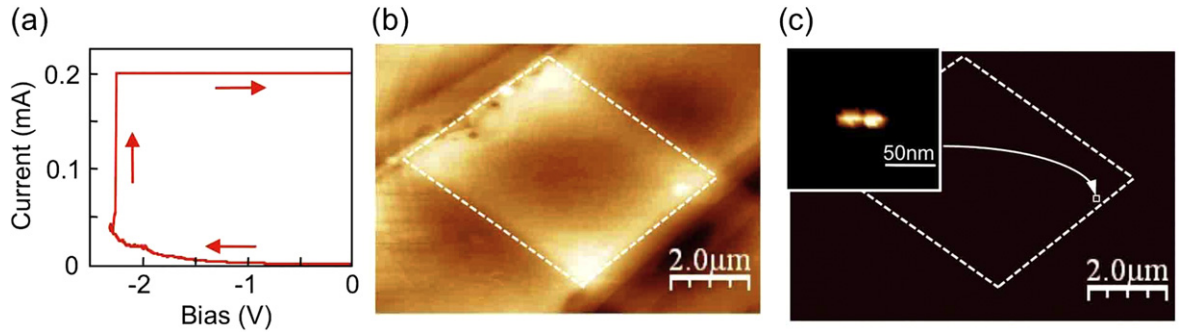

Figure 2. (a) Current–voltage sweep between the top and bottom electrodes for switching the device to a non-volatile ON-state. Bias was applied to the bottom Pt electrode while the top Cu electrode was grounded. (b) Topography image of the top electrode of the device. (c) Current image indicating a conducting point that corresponds to the position of a conducting filament. The double peak shape of the conducting point may reflect the surface morphology, since contact resistance between the cantilever and the surface also varies depending on surface morphology.

3. Results and discussion

First, we turned the device on by applying a negative bias to the bottom electrode while the top electrode was grounded. For this measurement, an Au(30 nm)/Cu(20 nm)/Ta_2O_5(15 nm)/Pt(30 nm) device was used. Figure 2(a) shows an *I*/*V* curve in the turning-on process, where the compliance current was set at 200 μA. The device was turned-on at −2.3 V and was kept at a non-volatile ON-state. The initial off resistance was typically greater than 10 GΩ and the on-resistance was approximately 100 Ω, which suggests that the resistance of the filament is much smaller in comparison to the resistance of the electrodes. Figures 2(b) and (c) show an AFM topography image and a current image for the device after the turning-on process. The diamond shaped area in the center of figure 2(b) corresponds to the device area, i.e., Au/Cu/Ta_2O_5/Pt. The device area is indicated by the white dashed lines in figure 2(c). As mentioned in section 2, Au (30 nm) is a protective layer. The current image, obtained with a bias of −150 mV applied to the bottom electrode, shows a single small conducting point in the whole device area, corresponding to the filament position. The area containing the conducting point is enlarged in the inset of figure 2(c).

To ensure that the conducting point corresponds to the actual filament position, the device was turned off once, and turned on again. Figures 3(a) and (b) are topographic and current images measured in the OFF-state at a position where the conductive point was observed in figure 2. It can be seen that the conducting point disappeared. *I*/*V* spectroscopy measured at the conducting point using a conductive cantilever clearly suggests the disappearance of the conductive channel between the top and bottom electrodes (figure 3(c)). Namely, no current was detected because the electric potential of the top electrode fell to ground level due to the disappearance of the conductive filament. Although the

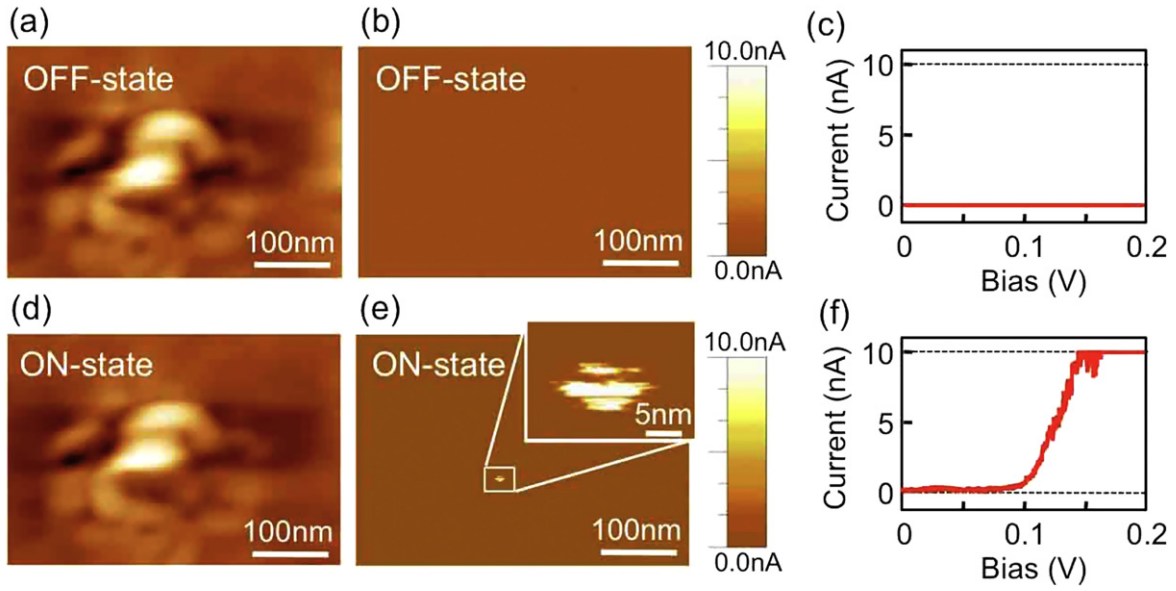

Figure 3. Topography and current images of the switching area of the device in its OFF-state (a), (b) and ON-state (d), (e). The corresponding current–voltage characteristics, obtained with an AFM Pt-tip at the conducting spot, are shown on the right-hand side of each image (c), (f).

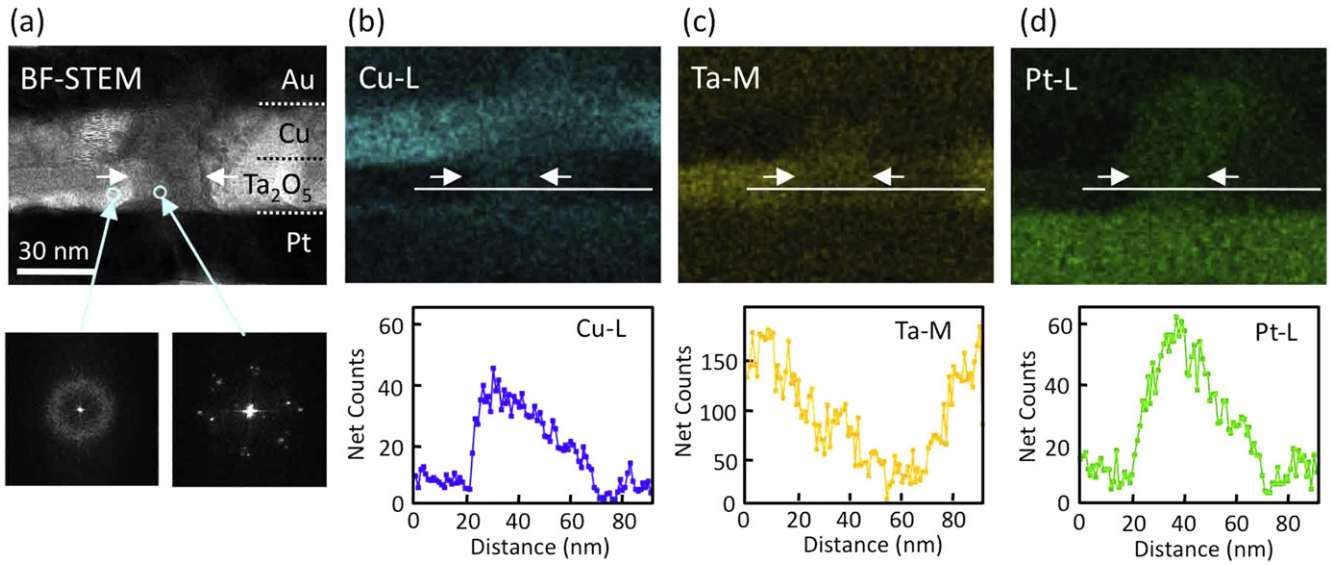

Figure 4. (a) TEM image of the cross-section of the device at the conducting point showing a thick conductive -filament formed between the top and bottom electrodes. FFT image of a region of the conductive-filament showing clear spots, indicating the presence of a crystalline phase. The neighboring area does not show any diffraction spots. EDX maps of (b) Cu, (c) Ta and (d) Pt in the conducting region. The profiles corresponding to the lines drawn on the EDX maps are shown below each map.

morphology of the area did not change, as can be seen by comparing the topographic images taken before (figure 3(a)) and after (figure 3(d)) the second turning-on, a conductive point appeared again in the same position in the large area ($5 \times 5\ \mu$m) of the device (figure 3(e)). *I*/*V* spectroscopy measured at the conducting point (figure 3(f)) clearly indicates the re-appearance of the conductive channel between the top and bottom electrodes. Namely, the electric potential at the conductive point increased due to the re-appearance of the conductive channel, enabling current to flow between the conductive cantilever and the top electrode. We expect that the nonlinearity in figure 3(f) is caused by the cantilever itself, because similar nonlinearity was observed on a directly biased metal surface.

TEM observation of the device cross-section at the conducting point revealed a wide (~40 nm) area containing Cu between the top and bottom electrodes, as shown in figure 4. The wide area is indicated by the white two arrows. A first Fourier transform (FFT) of the area shows some diffraction spots, suggesting the existence of crystalline metal, while the neighboring area does not show any diffraction spot, as shown in figure 4(a). The EDX map shows that the filament region contained Cu (figure 4(b)) and the concentration of Ta had decreased (figure 4(c)). The EDX line

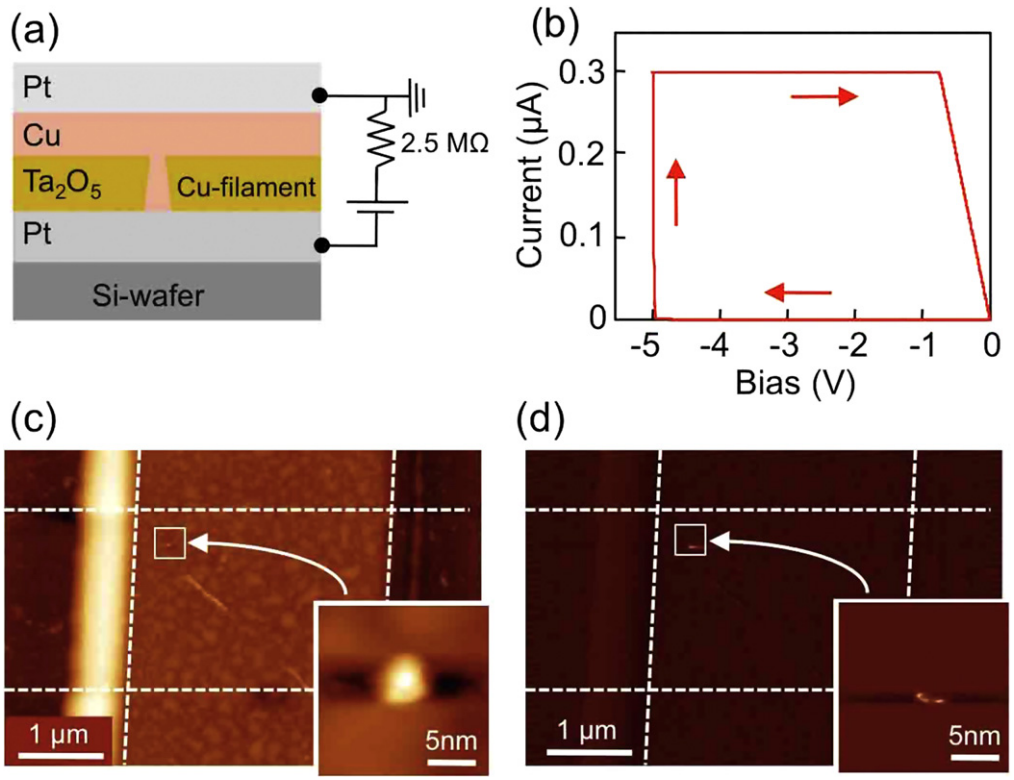

Figure 5. (a) Schematic of the turning-ON of a Cu/Ta_2O_5/Pt device with an external resistor, connected in series with the voltage source, acting as a current limiter. (b) Current–voltage sweep to turn-ON the device with the external resistor and a compliance current of 300 nA. (c) AFM topography image of the device top surface in its ON-state. A small protrusion appeared in the turning-on process. (d) Current image showing a conducting spot that corresponds to the Cu-filament formed inside the device. Insets are enlarged images for both topography and current.

profiles of Cu and Ta are shown below the respective EDX maps.

The above notwithstanding, the observed filament was much thicker than those reported and expected, e.g., 1–10 nm. We had thought that a large compliance current, i.e., 200 μA, would result in the formation of a thick filament. In addition, much larger current (transient current) flows momentarily through the device during the SET process due to the response-time delay of the instrument, which could also result in thick filament formation. Indeed, the SET time was found to be much shorter than the response time of the instrument [26]. Transient current is known to cause Joule-heating, which leads to physical damage and interferes with device operation, or even to cause complete device-breakdown. The EDX map and line profile of Pt (figure 4(d)) shows that Pt atoms were also brought into the filament region, which may be due to joule heating in the switching process. Therefore, limiting the current flow through the device is an important issue that needed to be addressed [27, 28].

We addressed the issue of limiting the current flow through the device by adding a series resistor to the measurement system, as shown schematically in figure 5(a), and using a compliance current at the lowest possible value (300 nA) necessary to obtain a non-volatile ON-state. The *I*/*V* curve in the turning-on process is shown in figure 5(b), where a Pt(5 nm)/Cu(20 nm)/Ta_2O_5(20 nm)/Pt(30 nm) device was used. The thicker Ta_2O_5 layer (20 nm) caused a larger bias (−5 V) for turning-on, while the bias for turning-on was −2.3 V for a 15 nm thick Ta_2O_5 layer (figure 2(a)).

The top surface of the device in its ON-state was scanned using the conductive-AFM setup to locate the position of the filament. The topography is shown in figure 5(c) and the current image, obtained with a bias of −500 mV applied to the bottom electrode, indicating a conducting spot on the top surface of the device, is shown in figure 5(d). Enlarged topography and current images are shown in the inset of each figure. In this device, the conductive point was also a single point in the large device area.

TEM observation of a cross-section of the device at the conducting point, shown in figure 6(a), revealed a dome-shaped structure at the bottom of the conductive region, as indicated by the white arrow. The area had a higher concentration of Cu and a lower concentration of Ta than the other area, as can be seen in the corresponding EDX maps of Cu (figure 6(b)) and Ta (figure 6(c)). Interestingly, Pt did not distribute in the Ta_2O_5 layer (figure 6(d)), thanks to the smaller compliance current that suppresses the joule heating effect. Figures 6(e) and (f) show a cross-section TEM image and an EDX map of an area far from the conducting point, which in turn show the existence of Cu ions along the interface between the bottom Pt electrode and the Ta_2O_5 layer.

The dome-shaped structure supports our understanding of the switching mechanism [12], although the part of the

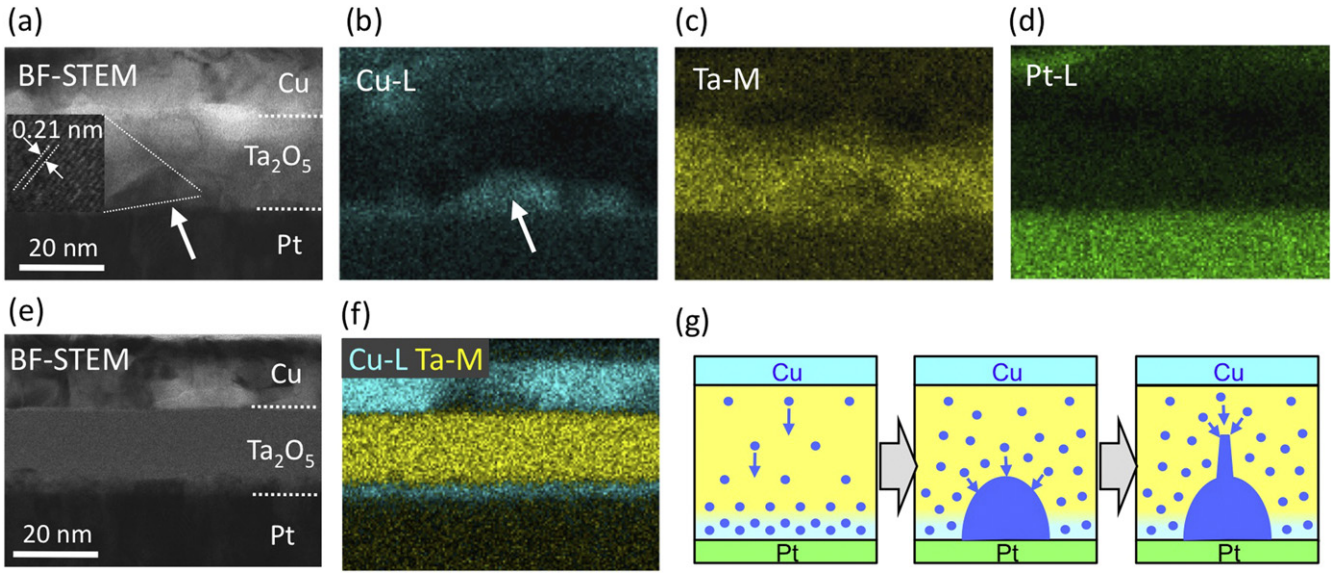

Figure 6. TEM observation of the cross-section of a Cu/Ta_2O_5/Pt device, at the conducting point, that was turned-ON with an external resistor to limit transient current. (a) TEM image of a conducting point showing a dome-shaped structure. Inset is an enlarged image of the dome-shaped area showing 0.21 nm fringes that correspond to a Cu(111) plane. EDX maps of (b) Cu, (c) Ta and (d) Pt at the conducting point. (e) TEM image of an area away from the conducting point, showing amorphous Ta_2O_5. (f) EDX map of Cu/Ta of the region away from the conducting point. (g) Schematics of a turning-on process.

filament connecting the top Cu-electrode was too thin to be resolved clearly due to EDX mapping instrumentation limitations. When a positive bias is applied to the Cu top electrode, anodic dissolution of Cu ions occurs at the Cu/Ta_2O_5 interface. These Cu ions migrate through the Ta_2O_5 matrix towards the bottom Pt electrode under the effect of the electric field that results from the applied bias (figure 6(g)-left). In the early stage of the turning-on process, Cu ions are supplied to the whole area of the Pt electrode, as can be seen in figure 6(f). Eventually, inhomogeneous nucleation of Cu occurs at the Ta_2O_5/Pt interface due to a cathodic deposition reaction (figure 6(g)-center), following which, Cu nuclei grow towards the top electrode and form a filament (figure 6(g)-right). There may be several nucleation sites where Cu nuclei might form and grow, but only a single complete filament is responsible for the ON-state. This is because as soon as a single filament completes the connection between the top and bottom electrodes, the resistance of the device drops down to about 100 Ω (the typical on-resistance value), which means that the resistance of the filament is smaller than the resistance of the electrodes. Therefore, on completion of the first filament, the electric field applied between the top and bottom electrodes suddenly decreases to such a small value that it prevents Cu ion migration and the further growth of other Cu nuclei. The current compliance system also stops further growth of other Cu nuclei by reducing the bias applied to the device when the current reaches the compliance level of the source meter. Once a filament is formed, growth and dissolution of the metal filament preferentially occur at the same point due to the electric field concentration on the formed nucleus. This is further supported by the fact that the AFM current images of the device top surface always showed a single conducting spot for the device.

4. Conclusion

In conclusion, we have demonstrated a simple and non-destructive method for locating the conducting filament of a Cu/Ta_2O_5/Pt device using a conductive-AFM. Generally, this method should be applicable for similar resistive switching devices, where the key-switching component is the formation and annihilation of a metal filament. Metal filaments, being Ohmic in nature, exhibit low resistance that enables their detection despite the presence of the top electrode of the device. Furthermore, TEM observations confirmed the formation of a Cu-filament in the switching area and elucidated the switching mechanism explaining the forming process and the effect of Joule heating. The results obtained in this study are important because Ta_2O_5-based atomic switches, being compatible with current CMOS fabrication processes, have great potential for technological applications.

Acknowledgments

This work was supported in part by JST/CREST and JST-EPSRC collaborative research project.

References

[1] Jeong D S, Thomas R, Katiyar R S, Scott J F, Kohlstedt H, Petraru A and Hwang C S 2012 Emerging memories: resistive switching mechanisms and current status *Rep. Prog. Phys.* **75** 076502

[2] Akinaga H and Shima H 2010 Resistive random access memory (ReRAM) based on metal oxides *Proc. IEEE* **98** 2237–51

[3] Waser R and Aono M 2007 Nanoionics-based resistive switching memories *Nat. Mater.* **6** 833–40

[4] Kim K M, Jeong D S and Hwang C S 2011 Nanofilamentary resistive switching in binary oxide system; a review on the present status and outlook *Nanotechnology* **22** 254002

[5] Valov I, Waser R, Jameson J R and Kozicki M N 2011 Electrochemical metallization memories—fundamentals, applications, prospects *Nanotechnology* **22** 254003

[6] Kwon D-H *et al* 2010 Atomic structure of conducting nanofilaments in TiO_2 resistive switching memory *Nat. Nanotechnology* **5** 148–53

[7] Yang J J, Pickett M D, Li X, Ohlberg D A A, Stewart D R and Williams R S 2008 Memristive switching mechanism for metal/oxide/metal nanodevices *Nat. Nanotechnology* **3** 429–33

[8] Lee M–J *et al* 2011 A fast, high-endurance and scalable non-volatile memory device made from asymmetric Ta_2O_{5-x}/TaO_{2-x} bilayer structures *Nat. Mater.* **10** 625–30

[9] Yang J J, Zhang M X, Strachan J P, Miao F, Pickett M D, Kelley R D, Medeiros-Ribeiro G and Williams R S 2010 High switching endurance in TaO_x memristive devices *Appl. Phys. Lett.* **97** 232102

[10] Russo U, Ielmini D, Cagli C and Lacaita A L 2009 Filament conduction and reset mechanism in NiO-based resistive-switching memory (RRAM) *IEEE Trans. Electron Devices* **56** 186–92

[11] Lin K-L, Hou T-H, Shieh J, Lin J-H, Chou C-T and Lee Y-J 2011 Electrode dependence of filament formation in HfO_2 resistive-switching memory *J. Appl. Phys.* **109** 084104

[12] Tsuruoka T, Terabe K, Hasegawa T and Aono M 2010 Forming and switching mechanisms of a cation-migration-based oxide resistive memory *Nanotechnology* **21** 425205

[13] Sakamoto T, Lister K, Banno N, Hasegawa T, Terabe K and Aono M 2007 Electronic transport in Ta_2O_5 resistive switch *Appl. Phys. Lett.* **91** 092110

[14] Schindler C, Staikov G and Waser R 2009 Electrodekinetics of Cu–SiO_2-based resistive switching cells: overcoming the voltage–time dilemma of electrochemical metallization memories *Appl. Phys. Lett.* **94** 072109

[15] Yang Y, Gao P, Gaba S, Chang T, Pan X and Lu W 2012 Observation of conducting filament growth in nanoscale resistive memories *Nat. Communication* **3** 732

[16] Tanaka H, Kinoshita K, Yoshihara M and Kishida S 2012 Correlation between filament distribution and resistive switching properties in resistive random access memory consisting of binary transition-metal oxides *AIP Adv.* **2** 022141

[17] Lee M H and Hwang C S 2011 Resistive switching memory: observations with scanning probe microscopy *Nanoscale* **3** 490–502

[18] Lee M H, Song S J, Kim K M, Kim G H, Seok J Y, Yoon J H and Hwang C S 2010 Scanning probe based observation of bipolar resistive switching NiO films *Appl. Phys. Lett.* **97** 062909

[19] Ahn S E *et al* 2008 Write current reduction in transition metal oxide based resistance change memory *Adv. Mater.* **20** 924–8

[20] Celano U, Chen Y Y, Wouters D J, Groeseneken G, Jurczak M and Vandervorst W 2013 Filament observation in metal-oxide resistive switching devices *Appl. Phys. Lett.* **102** 121602

[21] Miao F, Strachan J P, Yang J J, Zhang M-X, Goldfarb I, Torrezan A C, Eschbach P, Kelley R D, Medeiros-Ribeiro G and Williams R S 2011 Anatomy of a nanoscale conduction channel reveals the mechanism of a high-performance memristor *Adv. Mater.* **23** 5633–40

[22] Tsuruoka T, Terabe K, Hasegawa T and Aono M 2011 Temperature effects on the switching kinetics of a Cu–Ta_2O_5-based atomic switch *Nanotechnology* **22** 254013

[23] Tsuruoka T, Terabe K, Hasegawa T, Valov I, Waser R and Aono M 2012 Effects of moisture on the switching characteristics of oxide-based, gapless-type atomic switches *Adv. Funct. Mater.* **22** 70–7

[24] Tsuruoka T, Hasegawa T, Terabe K and Aono M 2012 Conductance quantization and synaptic behavior in a Ta_2O_5-based atomic switch *Nanotechnology* **23** 435705

[25] Tada M *et al* 2009 Highly scalable nonvolatile TiO_x/$TaSiO_y$ solid-electrolyte crossbar switch integrated in local interconnect for low power reconfigurable logic *IEDM Tech. Dig.* 943–6

[26] Tsuruoka T, Hasegawa T, Valov I, Waser R and Aono M 2013 Rate-limiting processes in the fast SET operation of a gapless-type Cu–Ta_2O_5 atomic switch *AIP Adv.* **3** 032114

[27] Lu Y M, Noman M, Chen W, Salvador P A, Bain J A and Skowronski M 2012 Elimination of high transient currents and electrode damage during electroformation of TiO_2-based resistive switching devices *J. Phys. D: Appl. Phys.* **45** 395101

[28] Lu Y M, Jiang W, Noman M, Bain J A, Salvador P A and Skowronski M 2011 Thermographic analysis of localized conductive channels in bipolar resistive switching devices *J. Phys. D: Appl. Phys.* **44** 185103